ACS OMEGA

Open Access

http://pubs.acs.org/journal/acsodf

Article

Flexible and Durable Direct Ink Writing 3D-Printed Conductive Fabrics for Smart Wearables

Zihui Zhao, Wangcheng Liu, and Hang Liu*

Cite This: *ACS Omega* 2025, 10, 14138−14149

Read Online

ACCESS | Metrics & More | Article Recommendations | Supporting Information

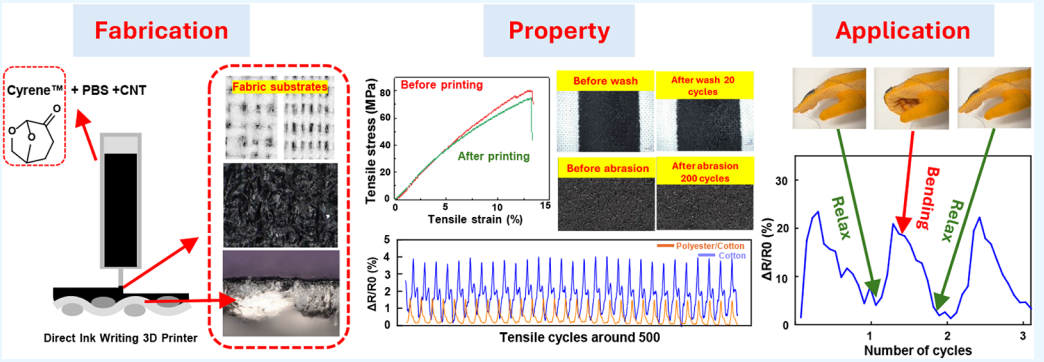

ABSTRACT: Functional fabrics have broad applications in smart wearables, offering diverse functions, such as sensing, energy harvesting, and actuation. The use of 3D printing to deposit functional materials onto textile fabrics has emerged as a transformative approach in smart wearable development due to the advantages it offers. However, achieving the desired functionalities while maintaining the fabric's flexibility, wearing comfort, washability, and durability of the printed material remains a challenge. In this study, direct ink writing (DIW) 3D printing technology was employed to print polybutylene succinate (PBS) solutions containing carbon nanotubes (CNTs) onto two types of fabrics. Various properties of the printed fabrics were assessed to examine the influence of printing solutions, fabric structures, and postprinting processes on printing performance. The printed fabrics exhibited excellent electrical conductivity, mechanical strength, gauge factor, and stability under repeated strains. These characteristics highlight their potential for use in smart wearable devices such as strain- and motion-detecting sensors. Analysis of the printed fabric morphologies revealed that factors such as fiber content, yarn structure, and surface roughness of the substrate fabric, along with the rheological properties and surface tension of the printing solution, played key roles in determining the wetting and penetration behaviors of the solution on the substrate. The solution's ability to penetrate and bond with fibers provided the printed fabrics with enhanced washability and abrasion resistance, demonstrating the advantages of DIW printing technology in developing textile-based sensors for smart wearables. Additionally, by using biobased and biodegradable nontoxic Cyrene as the solvent for processing, the printed fabric is safer for smart wearables, and the process is more environmentally friendly than commonly used toxic solvents for PBS.

1. INTRODUCTION

Smart wearables are a rapidly advancing field driven by innovations in sensor technology, manufacturing processes, and big data analytics. These devices, integrated into clothing or accessories, have the ability to monitor, track, and transmit various physiological and environmental data, providing valuable information for health, fitness, and lifestyle management.[1−3] For smart textiles, the techniques used to embed sensors and electronic devices within garments play a vital role in influencing the performance of the final products.[4] Traditional methods, such as sewing, gluing, or weaving functional parts (e.g., conductive threads or commercial sensors) directly onto fabrics, are commonly adopted.[5−7] These approaches often fall short in delivering multifunctionality and are constrained by the types of materials that can be used.[8,9] To address these limitations, in recent years, researchers have been developing functional composite fibers via fiber spinning and functional yarns via coating for fabric production with enhanced features, such as electrical conductivity.[10−14]

Another advancement in smart textiles is the direct application of functional materials onto a substrate through various coating and printing technologies, which combine the processes of manufacturing functional parts and integrating them with textile substrates into one step.[15−19] Among these,

Received: December 17, 2024
Revised: March 25, 2025
Accepted: March 26, 2025
Published: April 1, 2025

3D printing has emerged as a transformative technology due to its ability to process a wide range of materials, create intricate patterns, customize designs for individual needs, enable multifunctionality, and reduce waste during production.[20−23] This technology includes a range of methods, such as fused deposition modeling (FDM), direct ink writing (DIW), stereolithography (SLA), digital light processing (DLP), selective laser sintering (SLS), and laminated object manufacturing (LOM). They can deliver various materials, including molten polymers, viscous liquids, photocurable resins, and powder granules.[24,25] 3D printing enables the fabrication of complex patterns and the application of multifunctional materials, facilitating the creation of sophisticated smart wearable systems for health monitoring, motion tracking, or chemical detection.[26−34] It also improves the production time for small-scale parts, enhances energy efficiency, and minimizes waste. Studies have reported printing functional fillers onto elastomeric substrates, which are then attached to the skin using adhesives, wristbands, or straps for sensing.[28,35,36] Challenges involved in these technologies are that some adhesive components can cause skin irritation, and straps often struggle to achieve a snug fit, limiting long-term usage.[37−39] In response to consumer and market demands, researchers are developing 3D-printed textile-based smart wearables where sensors, electrodes, and circuits are printed directly onto traditional fabrics, aiming for seamless integration into everyday clothing for unobtrusive and continuous monitoring. The mainstream of related research focuses on FDM printing of elastic polymers.[40,41]

Although progress has been made, 3D printing of textile-based smart wearables still faces some challenges in achieving both functionalities and the required properties for daily wearing comfort and maintenance, including mechanical strength, flexibility, durability, and washability of the printed fabrics. Ideally, the printed layer is as flexible and stretchable as the textile substrate to maintain comfort and avoid peeling off during use and maintenance with repeated bending and abrasion. For long-term durability and washability, the printed layer is also required to have a strong bond with the substrate. Additionally, sustainability and cost-effectiveness are important considerations in modern manufacturing.[42] To achieve these features, the selection of 3D printing technology, functional printing material, and substrate is critical.

In this study, we investigated printing conductive materials on textile fabrics using DIW printing. DIW has a higher printing resolution than FDM and is less complex and costly than SLA, DLP, and other printing techniques.[41−43] The ability of DIW to print a solution is a significant advantage in smart wearable development, as various functional materials can be conveniently dispersed or dissolved in a solvent as the printing ink.[44] The process of preparing a solution is much simpler than preparing a filament for FDM printing. However, compared to a molten polymer, a solution has a higher flowability, which leads to a complex interaction between the printed solution and the fabric substrate. The solution's viscoelasticity, the fabric structures, and the compatibility between the printing material and the fabric all play important roles in affecting the printing process and the performance of the printed fabric.[45,46] There has been very limited information in the literature related to the DIW printing of smart wearables. Here, we used commercial textile fabrics as the printing substrate and CNT dispersed in poly(butylene succinate) (PBS) solution as the printing ink to develop conductive 3D-printed fabrics. The printability of various concentrations of printing inks on two different fabrics (a cotton fabric and a polyester/cotton blend fabric), inking penetration into the fabric, and the properties of the printed fabrics, including electrical conductivity, washability, and abrasion resistance, were evaluated. The influence of printing solution properties, fabric substrate, and postprinting processing was investigated, and the potential application of the printed fabrics as gesture detectors was demonstrated. A biobased and biodegradable solvent, dihydrolevoglucosenone (commercialized as Cyrene), was selected to dissolve PBS and disperse CNT in order to substitute commonly used toxic solvents for PBS processing. The rheological properties of solutions of PBS/CNT in Cyrene were evaluated to assess the processability of the solutions. In addition to the biodegradable nature of PBS, the use of Cyrene aligns with green chemistry principles and sustainable manufacturing practices, furthering the overall ecofriendly approach of this research.

2. MATERIALS AND METHODS

2.1. Materials. Two plain weave fabrics (Waverly Inspiration, USA), cotton/polyester blend (35%/65%) (CP) and unbleached muslin (100% cotton) (C), were used as the printing substrates. Multiwalled carbon nanotubes (CNTs, purity 98%, diameter = 100 μm, length = 20−200 μm), purchased from Sigma-Aldrich, were used as the conductive fillers. Cyrene (dihydrolevoglucosenone) was also purchased from Sigma-Aldrich. Poly(butylene succinate-*co*-adipate) (PBS) (FD92) was purchased from Mitsubishi Chemicals. All materials were used as received without any further treatment.

2.2. Printing Solution Preparation. The PBS and CNT blend solutions were prepared in two sequential steps. Initially, CNT was dispersed into Cyrene by intermittent ultrasonication (Branson SSE-1) at 20% amplitude for 20 min (∼5 °C). The PBS pellets were introduced into the CNT dispersions and dissolved with magnetic stirring at 80 °C for 12 h. The printed fabric properties of six solutions combining two CNT concentrations (1 and 2 wt %) and three PBS concentrations (15, 18, and 20 wt %) were evaluated based on their printability, as determined from preliminary studies. The solution was denoted as the PBS concentration − CNT concentration in the paper. For example, 15−1 means that the printing solution contained 15% PBS with 1% CNT.

2.3. Sample Printing. For DIW printing, the solution was transferred to a 10 mL syringe equipped with an 18-gauge needle and loaded onto the 3D printer (CulturES 3Ds, USA). The printing platform was preheated to 80 °C. A rectangular pattern with a size of 1 cm × 4 cm was printed on the substrate at a printing speed of 3 mm/s. After printing, the samples were immersed in DI water for 1 h to exchange and remove the Cyrene solvent, followed by drying in an 80 °C oven overnight. After that, the samples were hot-pressed at 80 °C for 120 s.

2.4. Measurements and Characterization. *2.4.1. Characterization of Ink for Printing.* The rheological properties of the solutions were evaluated with an oscillatory rheometer equipped with 25 mm parallel plates (TA Instruments, DHR-2). Steady shear viscosity at 25 and 60 °C was measured and recorded as a function of shear rate from 10^{-1} to 10^{2} s^{-1}. The gap between the parallel plates was 500 μm. The testing results were based on the average of three replicates. To calculate the shear rate (γ) of the solution flowing through the printing

https://doi.org/10.1021/acsomega.4c11367
ACS Omega 2025, 10, 14138−14149

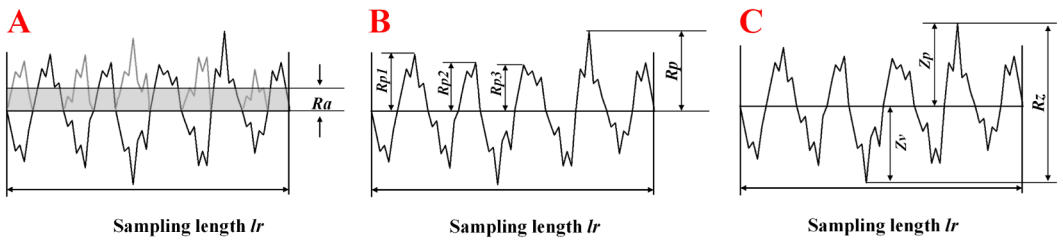

Figure 1. Calculation scheme for surface roughness, R_a (A), R_p (B), and R_z (C).

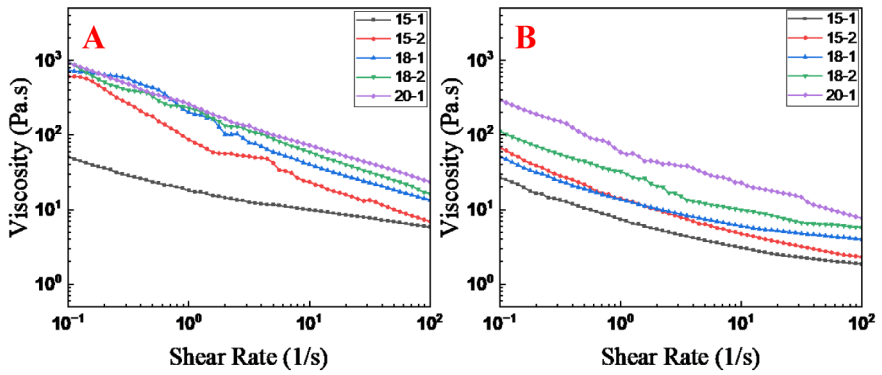

Figure 2. Viscosities of PBS−CNT solutions at 25 (A) and 60 °C (B).

needle based on the printing settings of this study, eq 1 was used:[47]

$$\gamma = \frac{4Q}{\pi r^3} \tag{1}$$

where Q is the volumetric flow rate calculated based on eq 2 and r is the nozzle radius of the needle.

$$Q = \frac{\pi C(\alpha D)^2}{4} \tag{2}$$

where C is the printing speed, D is the inner diameter of the needle, and α is the solution die swelling ratio.

In this study, the values of C and D were 3 and 0.84 mm, respectively. The die swelling α is generally between 1 and 1.5.[48] We adopted the value of 1.3 in the calculation. Therefore, Q was calculated as 2.76 mm^3/s and γ was 47.7 s^{-1}.

2.4.2. Printed Fabric Morphology and Structure Analysis. A digital optical microscope (Keyence VHX-7000) was used to take images of the surface and cross sections of the printed samples. Surface roughness data were automatically calculated by the software, including arithmetic mean roughness (R_a), the maximum profile peak height (R_p), and the maximum height of the profile (R_z). Their definitions and calculations are shown in Figure 1 and eqs 3−5 (ISO 4287-1996 section 4.2.1).

$$R_a = \frac{1}{lr}\int_0^{lr} |Z(x)|dx \tag{3}$$

$$R_p = \max(Z(x)) \tag{4}$$

where $Z(x)$ refers to the values of the surface profile heights (ordinates) within the given sampling length.

$$R_z = Z_p + Z_v \tag{5}$$

where Z_p is the height of the highest peak, and Z_v is the largest profile valley depth within a sampling length.

The nanoscale surface measurement of the unprinted fabrics was measured using an atomic force microscope (Veeco Metrology MMAFMLN).

2.4.3. Electrical Resistivity Test. The electrical resistivity of the samples was measured using a JG constant current resistivity apparatus (Model SZT-C) following the methodology proposed by Smits.[49] This device incorporates a four-point cylindrical probe arrangement, where the probes are linearly positioned with equal spacing of 1.016 mm. Each probe with a radius of 100 μm facilitates the passage of a constant current (I) through the outer probes, and a voltmeter measures the voltage (V) across the inner probes. The resistivities of the samples were derived by applying Ohm's Law.

2.4.4. Solution Wettability on the Fabrics. The contact angles (CAs) of water, Cyrene, and PBS−CNT solutions on the two fabric substrates were measured by using a VCA Optima Video Contact Angle System (AST Products Co., USA). The CAs were recorded at 0, 5, 60, and 300 s after the solution droplet contacted the sample surface. The measurement was performed at 21 °C and repeated three times.

2.4.5. Mechanical Properties. Tensile testing and a tensile cyclic test of the printed sample were performed on a universal testing machine (Instron 5565) equipped with a 5 kN load cell following the ASTM 5035 Standard Test Method for Breaking Force and Elongation of Textile Fabrics (strip method). The wash test was performed under home laundering conditions using a washing machine (Frigidaire FER21AS2) and a drying machine (Frigidaire FWX833AS1) following the AATCC LP1-2021 Home Laundering: Machine Washing. The abrasion test was performed on a universal wear tester following the ASTM D3885 Standard Test Method for Abrasion Resistance of Textile Fabrics (Flexing and Abrasion Method) for 200 cycles. All tests were repeated three times to calculate the mean and standard deviation.

2.4.6. Sensing Performance Measurement. The resistivity change of the printed fabric (1 cm × 4 cm) under various

https://doi.org/10.1021/acsomega.4c11367
ACS Omega 2025, 10, 14138−14149

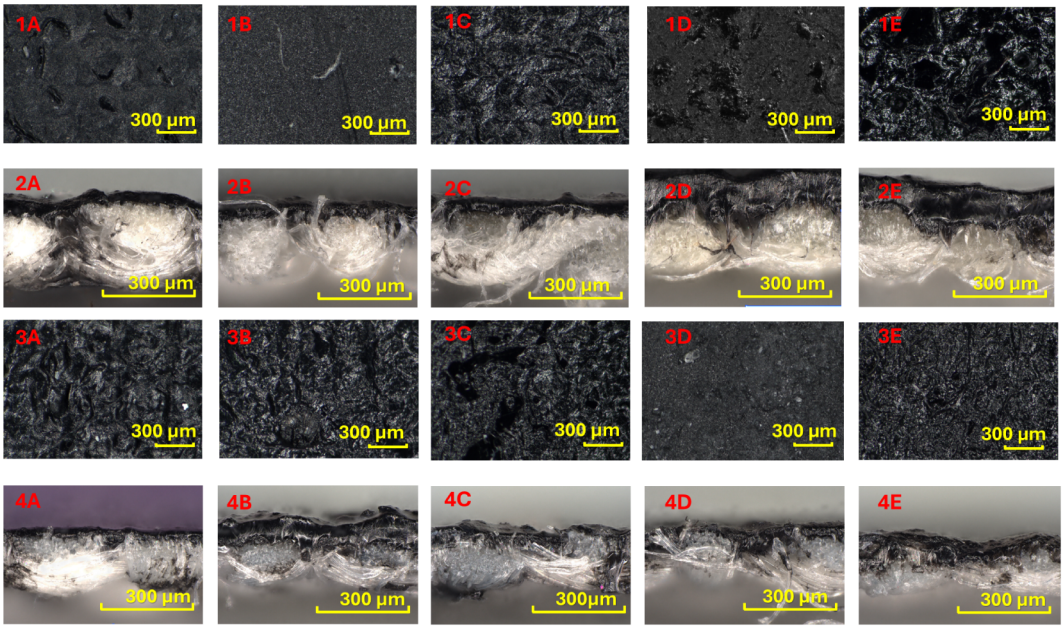

Figure 3. Surface (1s and 3s) and cross-sectional (2s and 4s) images of printed cotton (1s and 2s) and polyester/cotton (3s and 4s) fabrics with the five solutions (A: 15-1; B: 15-2; C: 18-1; D: 18-2; E: 20-1).

strains was evaluated on the Instron testing machine with a multimeter (Keithley 34461A, KEYSIGHT Technology, USA) connected to the printed fabric. The multimeter was in a two-probe testing mode (100 V) with direct current (DC). The relative resistance is defined according to eq 6:[50]

$$\frac{\Delta R}{R_0} = \frac{R - R_0}{R_0} \times 100\% \quad (6)$$

where R_0 and R are the resistance values of the original and stretched PBS−CNT printed samples, respectively.

To evaluate the gesture detection functionality of the printed fabric, a 15-1 printed cotton fabric of size 1 cm × 4 cm was sewn onto the proximal interphalangeal joint area of a glove's index finger. The Keithley 34461A multimeter was connected to the printed fabric to measure resistivity changes as the wearer repeatedly bent and straightened the index finger 10 times.

3. RESULTS AND DISCUSSION

3.1. Printing Solution Properties. Six solutions were prepared based on three loads of PBS (15, 18, and 20%) and two concentrations of CNT (1 and 2%). With 20% PBS, the solution became too viscous to evenly disperse 2% CNT. Therefore, this formulation was not adopted in the following study. The viscosity of the remaining five solutions as a function of the shear rate is shown in Figure 2. All solutions exhibited shear-thinning behavior, where the apparent viscosity decreased significantly as the shear rate increased from 1×10^{-1} to 1×10^{2} s^{-1}. Higher polymer concentrations led to increased viscosity, following the general relationship between polymer concentration and solution viscosity.[51] At a consistent polymer load, higher CNT concentrations also resulted in increased solution viscosity. For successful DIW printing, polymer solutions need to exhibit shear-thinning behavior and resemble a liquid during extrusion, maintain structural integrity immediately after extrusion, and quickly transition to a solid state under zero shear.[52,53] As shown in Figure 2, the viscosities of the five solutions at a shear rate of 47.7 s^{-1} (which is the shear rate during printing in this study, as calculated in Section 2.4.1) were 6.8, 10.0, 18.4, 24.6, and 33.7 Pa·s at 25 °C, and 2.1, 2.7, 4.5, 6.4, and 11.1 Pa·s at 60 °C for the 15-1, 15-2, 18-1, 18-2, and 20-1 solutions, respectively. The values fell within the range of printable solution viscosities, which is 0.1−10^3 Pa·s according to the literature.[54] The rheological results demonstrated that the biobased and biodegradable solvent Cyrene is a viable alternative to commonly used toxic organic solvents for processing PBS (e.g., chloroform and tetrahydrofuran).

3.2. Ink−Substrate Interaction and Printed Fabric Morphology. In contrast to FDM printing, where polymers typically remain on the substrate's surface, the surface and cross-sectional images of the printed and pressed fabrics (Figure 3) show that the solution not only spread evenly across the fabric surface but also penetrated into the fabric and yarn. Additionally, the levels of penetration on the two types of fabrics were different. The solution flowed deeper into the CP fabric and filled the spaces not only between yarns but also between fibers within a yarn. In comparison, the solution penetration into the cotton fabric was primarily between yarns, with limited infiltration into the yarn structure, i.e., between fibers. During printing, once the solution was deposited onto the fabric surface, its movement involved spreading/wetting across the fabric surface in the 2D plane and wicking into the fabric's depth in the third dimension. Several fabric properties played a role in this process, including the fabric surface energy, the polarity of the fibers in the fabric, and the surface roughness of the fabric and fibers.

Polyester is a long-chain polymer composed mainly of nonpolar aromatic rings, which lead to its low surface energy and hydrophobicity. The surface energy of polyester fabrics ranges between 30 and 50 mJ/m^2,[55] while that of cotton fabrics ranges from 50 to 80 mJ/m^2.[56] Although polyester fabrics repel water due to their low surface energy and hydrophobicity, they have a higher affinity and wettability for low surface tension liquids, such as Cyrene, which has a surface tension of 33.6

https://doi.org/10.1021/acsomega.4c11367
ACS Omega 2025, 10, 14138−14149

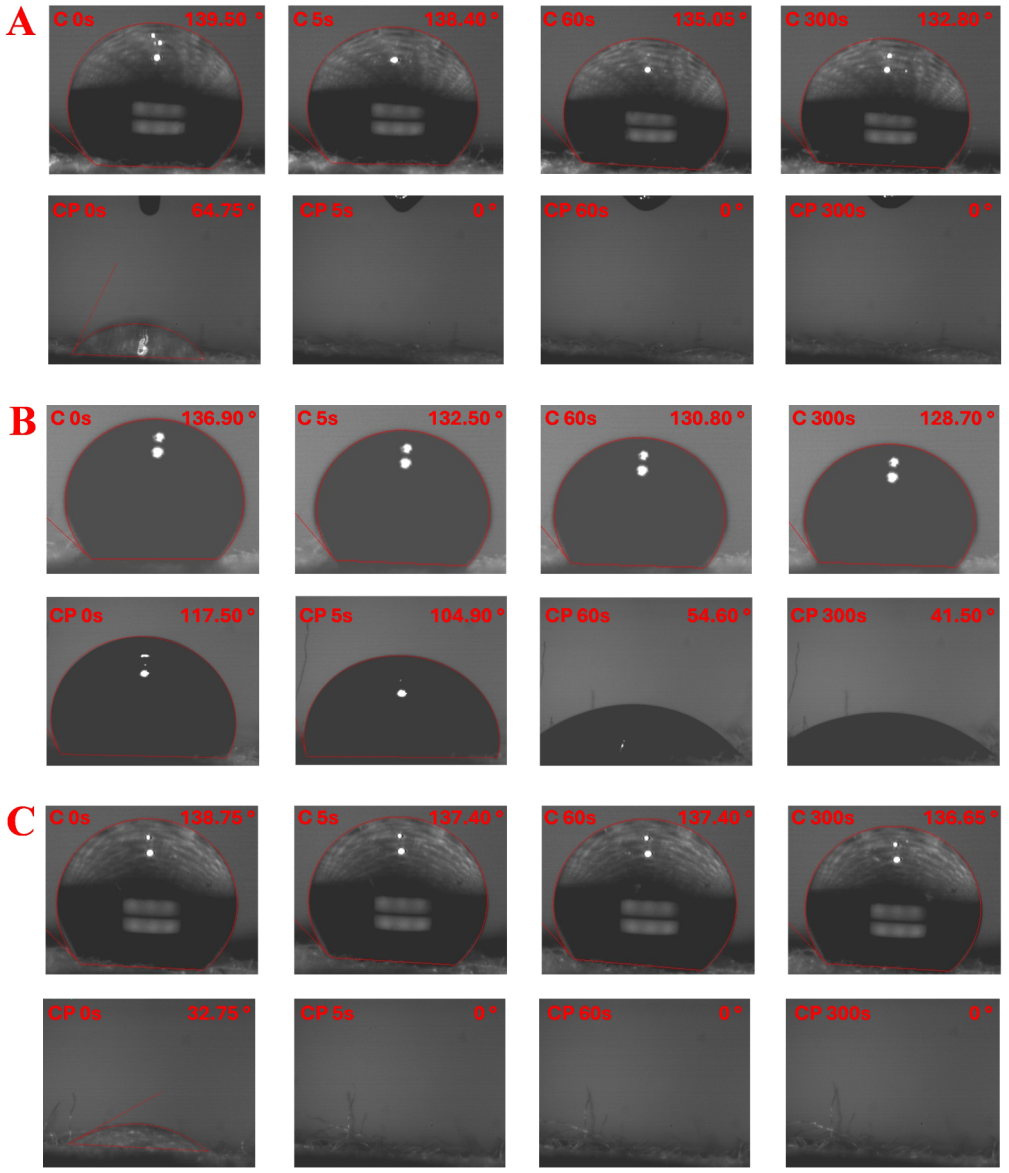

Figure 4. Contact angle of Cyrene (A), 15-1 PBS−CNT solution (B), and water (C) on the cotton and polyester/cotton blend fabrics.

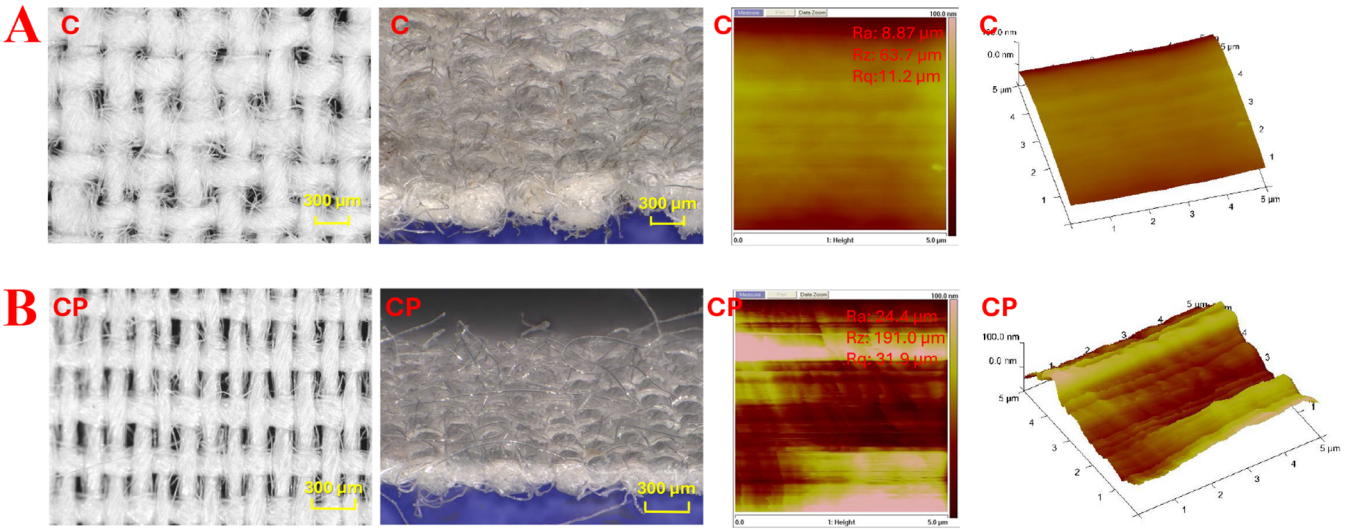

Figure 5. Fabric substrates and relative surface roughness: (A) cotton (C) and (B) polyester/cotton (CP) blend fabrics.

https://doi.org/10.1021/acsomega.4c11367
ACS Omega 2025, 10, 14138−14149

mN/m compared to water at 72.5 mN/m.[57,58] As shown in Figure 4A, the CP blend fabric readily absorbed Cyrene. The initial contact angle of Cyrene on the CP blend fabric upon contact was 64.75°, reducing to 0° within 5 s. In contrast, the contact angles on the cotton fabric were 139.50° initially and 132.80° after 300 s. The contact angle test of the 15-1 PBS/CNT printing solution on the two fabrics showed similar results; i.e., the CP blend fabric had much lower contact angles than the cotton fabric (Figure 4B).

Ink penetration can also be affected by the capillary effect or wicking within the fabrics. A smoother fabric surface, resulting from more uniform fiber arrangements, increases the continuity of capillaries formed by the fibers within the yarn, thereby enhancing the wicking effect. The CP fabric had smooth polyester fibers, and the yarn twist was low. Both factors promoted solution penetration into the yarns and along the fiber surfaces via wicking to fill the fabric interstices. In contrast, the cotton fabric exhibited reduced wicking due to its higher yarn twist and less organized fiber arrangement, which increased the tortuosity of the pores.[59,60] This reduced continuity impeded capillary action, leading to less solution penetration. As a result, the solidified PBS/CNT layer on the surface of the polyester fabric was thinner than that of the cotton fabric. The layer thickness difference was especially obvious for higher PBS concentrations and solution viscosities, i.e., 15-2 and 18-1.

Another factor that influences wetting is the fabric's surface roughness. Various studies have shown that rougher surfaces increase contact angles, particularly with highly polar liquids.[61−64] The cotton fabric used in this study contained coarse yarns with a low twist, and short cotton fiber ends protruded from the fabric surface plane, creating a fuzzy appearance. As measured by AFM (Figure 5), the surface roughness of the cotton fabric was significantly higher than that of the CP blend fabric, with average profile values (R_a), peak valley heights (R_z), and root-mean-square profile values (R_q) of 24.4, 191.0, and 31.9 μm, respectively, compared to 8.87, 63.7, and 11.2 μm for the CP blend fabric. The fuzzy fiber layer increased the fractional contact area between water and air, acting as a cushion that supported liquid drops and prevented them from spreading on the surface. Therefore, the cotton fabric exhibited high contact angles, even with water (Figure 3C). It is worth noting that the water droplets could remain on the cotton fabric surface for several minutes. However, once the static state was disrupted, water was quickly absorbed by the fabric, demonstrating the hydrophilic nature of the cotton fibers. The higher wettability of the printing solution on the CP fabric affected not only its spreading but also its penetration into the fabric.

Post-treatment hot pressing was found to have a significant influence on surface smoothness and conductivity. As shown in Figure 3, the surface and cross-sectional images reveal noticeable improvements after the pressing process. A comparison of pre- and postpressed printed fabrics is provided in Figure S1. The prepressed samples exhibited rough surfaces with voids that were eliminated after the hot press, resulting in a flatter surface. This flattening was evidenced by increased leveling of the yarns in the fabric and roughness measurements. After hot pressing, the mean roughness (R_a), maximum roughness (R_z), and profile peak height (R_p) of the printed fabric were reduced from 127.93 μm, 643.35 μm, and 446.13 μm to 66.52 μm, 275.06 μm, and 154.86 μm, respectively. Since the temperature used for the hot press (80 °C) was slightly lower than the melting point of PBS (90−100 °C), the internal stresses of softened PBS and fabrics were relaxed across the fabric surface and within the yarn interstices, which likely also improved the adhesion of the ink to the fabric through enhanced physical bonding. Additionally, the pressing process removed voids and air bubbles within the printed layer, contributing to a smoother surface.

3.3. Tensile Properties of the Printed Fabrics. The influence of printing on the mechanical strength of the fabrics was evaluated through tensile testing. The original cotton fabric had a tensile strength of 23.80 MPa and a tensile strain of 10.8% (Table 1). In most cases, printing enhanced the tensile strength and strain, except for the 15-1 solution. For the CP fabric, the tensile strength was 78.95 MPa, and the elongation was 12.67% before printing. After printing, the average tensile strength decreased slightly, while elongation increased. These results align with expectations, as PBS is a ductile polymer with tensile strength higher than that of the cotton fabric but lower than that of the polyester blend fabric. Additionally, the presence of CNT may have contributed to the strength increase in the PBS-printed layer on the cotton fabric. The stress−strain curves of the printed samples were smooth and continuous, indicating strong adhesion between the printed layer and the textile substrate (Figure 6).

Table 1. Tensile Properties of the Unprinted and Printed Fabrics

Fabric	Tensile strength (MPa)	Tensile strain (%)
C before printing	23.80 ± 1.76	10.80 ± 0.64
C 15-1	22.68 ± 1.80	16.39 ± 0.94
C 15-2	33.05 ± 2.44	24.02 ± 3.51
C 18-1	27.22 ± 2.74	12.01 ± 0.16
C 18-2	36.31 ± 3.65	18.17 ± 2.96
C 20-1	38.36 ± 2.15	13.67 ± 1.43
CP before printing	78.95 ± 1.75	12.67 ± 0.60
CP 15-1	73.74 ± 6.20	17.58 ± 2.41
CP 15-2	74.56 ± 0.02	14.21 ± 0.02
CP 18-1	75.48 ± 1.49	13.48 ± 0.88
CP 18-2	75.57 ± 1.36	14.16 ± 0.09
CP 20-1	73.68 ± 6.01	17.34 ± 0.12

3.4. Electrical Resistance and Sensitivity of the Printed Fabric. The electrical resistivity of the printed fabrics is listed in Table 2. The fabric resistivity was in the range of several kiloohms, from 1.56 to 5.56 KΩ. The influence of CNT and PBS concentrations followed general trends; i.e., higher

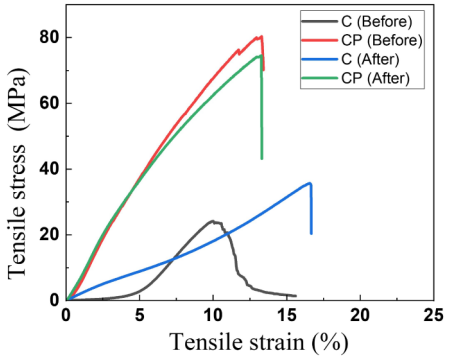

Figure 6. Stress−strain curves of the fabrics before and after printing.

https://doi.org/10.1021/acsomega.4c11367
ACS Omega 2025, 10, 14138−14149

Table 2. Gauge Factors of the Printed Fabrics at 2% and 5% of Strains

	C					CP				
Printed Fabrics	15-1	15-2	18-1	18-2	20-1	15-1	15-2	18-1	18-2	20-1
2%	4.8	9.0	6.5	2.3	25.5	10.4	14.5	14.1	15.6	60.5
5%	10.6	10.6	5.5	6.6	11.2	7.2	6.4	2.3	3.0	25.5

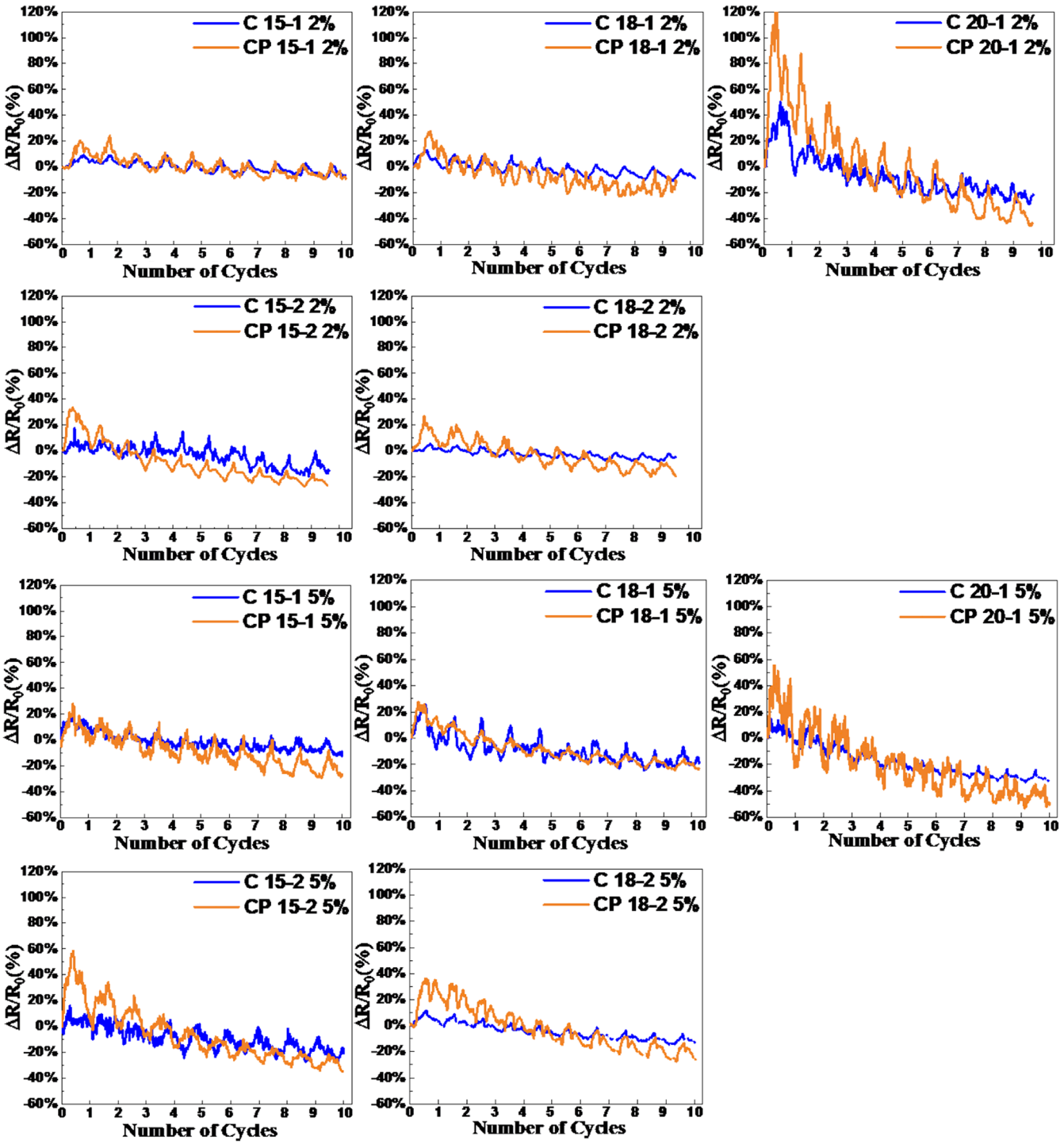

Figure 7. Relative resistance of printed fabrics under 2% and 5% strain for 10 cycles.

CNT concentration enhanced fabric conductivity, while increased polymer concentration decreased conductivity when CNT levels were constant. The conductivity change under fabric tensile deformation is crucial for determining the suitability of printed fabrics for applications like strain sensors or motion detectors.[65] To evaluate this, cyclic strains of 2% and 5% were applied to assess the relative resistivity of the printed fabrics. Figure 7 shows the relative resistivity during

https://doi.org/10.1021/acsomega.4c11367
ACS Omega 2025, 10, 14138−14149

the first 10 cycles. For both fabrics printed with different solution formulations, the relative resistivity displayed patterns similar to those synchronized with the strain cycles. Under each strain cycle, the relative resistivity increased with strain and then decreased as the load was removed, creating relative resistivity peaks. However, the amplitude of the peaks and the overall fabric resistance varied between the two fabrics. The cotton fabric had lower relative resistivity peaks in comparison to the CP fabric. The peak amplitude for CP decreased after the first several cycles. The trend was even more pronounced at 5% strain than at 2%. These differences likely stem from the yarn and fabric structural characteristics of the two fabrics. The strain−stress curves of the fabrics in Figure 6 showed that the cotton fabric had a gentle slope at strains below 5%, indicating greater extensibility and lower resistance to deformation due to the loose yarn and fabric structures. While for the CP blend fabric, the yarns had fewer twists and were more compact, leading to lower extensibility and higher resistance to deformation. Under small strains, the elongation of the cotton fabric mainly resulted from the straightening of the yarns rather than yarn elongation. Therefore, the influence on the printed layer was smaller than that in the CP blend fabric. This can also explain the overall stable fabric resistivity after stretching in the cotton fabric compared with the CP blend fabric.

Gauge factors, which reflect the sensitivity of strain sensors, were calculated based on the first strain cycle (Table 2). At 2% strain, the gauge factors of CP blend fabric ranged between 5.5 and 60.5 across the different printing formulations, significantly higher than those of the cotton fabric, ranging from 2.3 to 25.5. These gauge factors exceed those reported for FDM 3D-printed polymer-based strain sensors in the literature. For example, gauge factors up to 4.5 at 35% strain were reported for acrylonitrile butadiene styrene-based sensors,[66] while carbon black/carbon nanotubes/thermoplastic polyurethane sensors exhibited gauge factors ranging from 10 to 35.9 at 60% to 150% strains.[67] In practical applications, the stable 100% cotton-based sensor is well-suited for continuous health monitoring such as tracking heart rate, respiratory rate, and other physiological parameters. Meanwhile, the high sensitivity of the CP blend fabric makes it ideal for applications requiring the detection of small, precise movements such as gesture recognition systems.

Figure 7 also illustrates a general downward trend in the overall relative resistivity patterns, meaning that the conductivity of the printed fabrics improved after repeated stretching, particularly for the CP blend fabric. This interesting finding, contrary to the anticipated increase in resistivity, may be attributed to enhanced CNT alignment during stretching. Previous research has shown that CNT orientation within a polymer matrix significantly enhances electrical conductivity,[67−69] a phenomenon also observed with graphene coatings on fabrics.[70]

Figure 8 shows the relative resistivity of the printed fabrics after 500 cycles at 2% strain. The tested CP blend fabric demonstrated a 50% reduction in resistance compared to its initial resistance. The relative resistance dropped from 5% to 4%. On the other hand, the 100% cotton fabric showed a 29.5% decrease in resistance, with relative resistance dropping from 16% to 1% (Figure 8). The changes in relative resistance over the last 100 cycles are shown in Figure S2, which demonstrate the long-term stability of both printed fabrics.

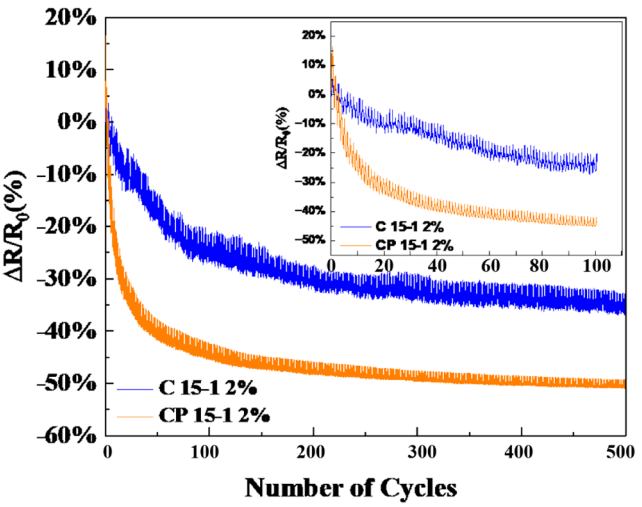

Figure 8. Relative resistance of the printed fabrics under 2% strain for 500 cycles. The inset shows the relative resistance of the first 100 cycles.

3.5. Washability and Abrasion Resistance of the Printed Fabrics. The practical application of printed fabric for smart wearables requires that both the printed material and electrical properties withstand washing and abrasion. The washability of 3D-printed smart wearables on two different fabric types was assessed by using the AATCC LP1-2021 standard. Despite a slight increase in electrical resistance observed in the 15-1 cotton fabric group and the 15-1 and 18-1 CP blend groups, all printing groups exhibited relatively stable resistivity after 20 washing and drying cycles (Figure 9 and Table 3). Additionally, no visible changes to the fabric surface were observed after the 20 cycles (Figure S3). This finding demonstrated the exceptional washability of the printed fabrics, which can eliminate the need for postprinting finishes. In line with the washability results, the printed fabric also exhibited exceptional flex abrasion resistance and flexibility. After 200 abrasion cycles, neither the electrical resistivity nor the fabric surface showed significant changes (Figure S4). No surface scratches or cracks were observed, as the smooth PBS layer effectively minimized wear and offered flexibility, enhancing the printed fabric's durability under flex abrasion. These results underscore the advantages of DIW printing, which effectively integrates the printed material into the fabric and becomes part of the fabric structure. Additionally, PBS contributed significantly by providing ductility, which afforded the printed layer great flexibility and the needed durability, ensuring its suitability for real-world applications.

3.6. Performance of Printed Fabric as a Motion Detector. To evaluate the performance of the 3D-printed fabrics as wearable sensors for movement detection, the 15-1 printed cotton fabric was directly attached to a glove to collect signals generated by finger bending, as displayed in Figure 10. The resistivity increased as the finger flexed, reaching a maximum change of 20−25% at the largest bending angle and then gradually returned to almost the baseline as the finger straightened. The cycle length corresponded to the speed of finger movement; i.e., slower finger movements resulted in wider peaks, while faster movements produced narrower peaks. These results demonstrate the potential of the printed fabric to function as a motion-detecting sensor, with both movement

https://doi.org/10.1021/acsomega.4c11367
ACS Omega 2025, 10, 14138−14149

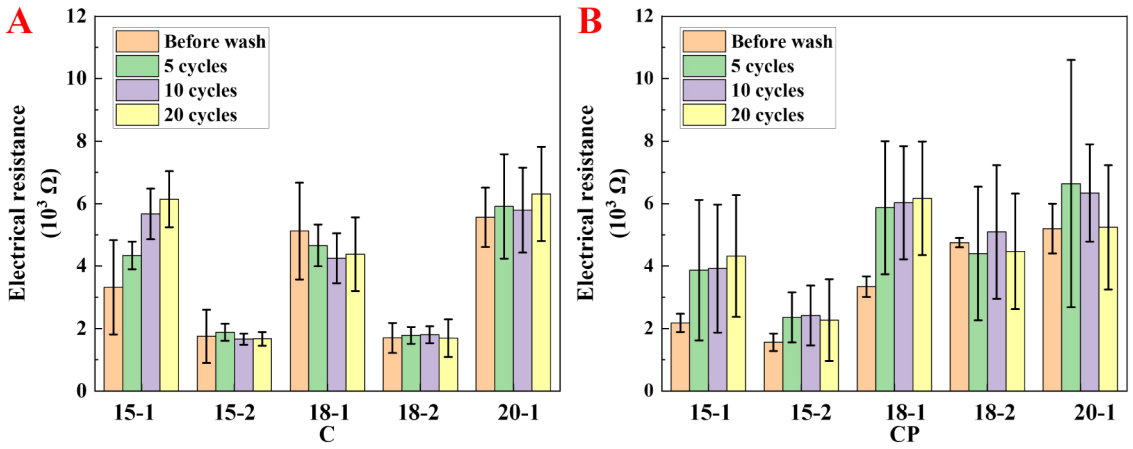

Figure 9. Electrical resistance after repeated washing of the cotton (A) and CP fabrics (B).

Table 3. Resistivity of the Printed Fabric Samples after Washing

Fabric	Before (10^3 Ω)	1st cycle (10^3 Ω)	5th cycles (10^3 Ω)	10th cycles (10^3 Ω)	20th cycles (10^3 Ω)
C 15-1	3.32 ± 1.51	3.71 ± 1.18	4.34 ± 0.44	5.67 ± 0.81	6.14 ± 0.90
C 15-2	1.75 ± 0.85	1.43 ± 0.31	1.88 ± 0.27	1.66 ± 0.18	1.67 ± 0.22
C 18-1	5.12 ± 1.55	4.92 ± 1.94	4.66 ± 0.67	4.26 ± 0.8	4.38 ± 1.18
C 18-2	1.70 ± 0.48	1.73 ± 0.17	1.78 ± 0.27	1.8 ± 0.27	1.69 ± 0.6
C 20-1	5.56 ± 0.95	5.99 ± 1.61	5.91 ± 1.67	5.79 ± 1.36	6.31 ± 1.51
CP 15-1	2.18 ± 0.29	2.98 ± 0.54	3.87 ± 2.25	3.92 ± 2.05	4.32 ± 1.95
CP 15-2	1.56 ± 0.28	1.71 ± 0.68	2.36 ± 0.80	2.42 ± 0.96	2.27 ± 1.31
CP 18-1	3.34 ± 0.33	3.32 ± 0.67	5.87 ± 2.13	6.03 ± 1.81	6.17 ± 1.82
CP 18-2	4.75 ± 0.15	5.39 ± 0.22	4.40 ± 2.14	5.09 ± 2.14	4.47 ± 1.85
CP 20-1	5.20 ± 0.80	5.57 ± 1.68	6.64 ± 3.96	6.34 ± 1.56	5.24 ± 1.99

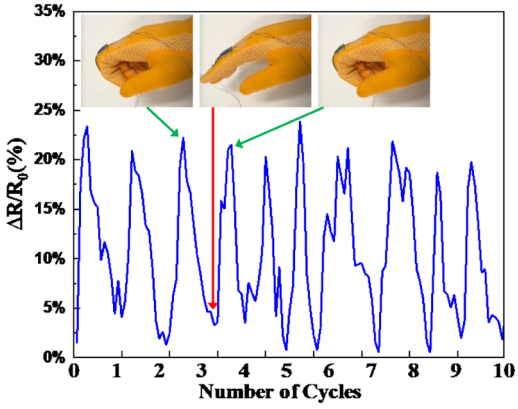

Figure 10. Electric signal response to finger bending.

speed and extent being captured through variations in the width and amplitude of the resistance curves.

4. CONCLUSION

In this study, textile-based flexible conductive fabrics were successfully developed using direct ink writing 3D printing technology. A biobased green solvent, Cyrene, was utilized to dissolve PBS for the preparation of printing solutions with CNT incorporated as the conductive filler. The rheological behavior of the solutions and the properties of the printed fabrics were thoroughly evaluated. The printed fabrics demonstrated great electrical conductivity, mechanical strength, gauge factor, and relative resistivity under repeated strains along with excellent abrasion resistance and washability. These attributes afforded the fabrics significant potential for use in smart wearable devices such as strain- and motion-detecting sensors. Analysis of the printed fabric surface and cross-sectional morphologies revealed that the fiber content, yarn structure, and surface roughness of the substrate fabric, in addition to the rheological properties and surface tension of the printing solution, played key roles in influencing the wetting and penetration behavior of the solution on the substrate. The penetration of the solution into the fabric between yarns and even between fibers within the yarns largely enhanced the durability of the printed layer, contributing to its great abrasion resistance and washability. The two fabrics examined here, i.e., the 100% cotton fabric and the 65% polyester and 35% cotton blend fabric, displayed different relative resistance responses under small strains (2% and 5%), showcasing their potential for various applications in strain and motion sensor technologies. The study underscores the advantages of DIW printing technology in the development of textile-based sensors for smart wearables with both advanced functions and required durability and flexibility, providing daily wearing comfort and easy maintenance.

■ ASSOCIATED CONTENT

Data Availability Statement

The authors confirm that the data supporting the findings of this study are available within the article and its Supporting Information. Raw data supporting the findings of this study are available from the corresponding author upon reasonable request.

Supporting Information

The Supporting Information is available free of charge at https://pubs.acs.org/doi/10.1021/acsomega.4c11367.

https://doi.org/10.1021/acsomega.4c11367
ACS Omega 2025, 10, 14138−14149

Surface and cross-sectional images of the printed cotton fabrics before and after hot press (Figure S1); relative resistance of the printed fabrics under 2% strain from 400 to 500 cycles showing the stabilized relative resistivity (Figure S2); digital microscope images of printed cotton fabrics before (A) and after (B) 20 washes (Figure S3); digital microscope images of printed CP fabrics before (A) and after (B) 200 cycles of abrasion (Figure S4) (PDF)

AUTHOR INFORMATION

Corresponding Author

Hang Liu − *Department of Apparel Merchandising, Design and Textiles, Washington State University, Pullman, Washington 99164, United States; Composite Materials and Engineering Center, Washington State University, Pullman, Washington 99164, United States;* orcid.org/0000-0002-8598-9406; Email: hangliu@wsu.edu

Authors

Zihui Zhao − *Department of Apparel Merchandising, Design and Textiles, Washington State University, Pullman, Washington 99164, United States*

Wangcheng Liu − *Composite Materials and Engineering Center, Washington State University, Pullman, Washington 99164, United States*

Complete contact information is available at: https://pubs.acs.org/10.1021/acsomega.4c11367

Author Contributions

Z.Z.: formal analysis, investigation, methodology, writing—original draft, writing—review and editing. W.L.: methodology, validation, writing—review and editing. H.L.: conceptualization, funding acquisition, methodology, project administration, supervision, validation, writing—original draft, writing—review and editing.

Notes

Any opinions, findings, and conclusions or recommendations expressed in this material are those of the author(s) and do not necessarily reflect the views of the National Science Foundation.

The authors declare no competing financial interest.

ACKNOWLEDGMENTS

This material is based on work supported by the National Science Foundation under Grant 2145468. W.L. is a postdoctoral research fellow supported by the Washington Research Foundation.

REFERENCES

(1) Chen, M.; Ma, Y.; Song, J.; Lai, C.-F.; Hu, B. Smart Clothing: Connecting Human with Clouds and Big Data for Sustainable Health Monitoring, Mob. *Netw. Appl.* **2016**, *21*, 825−845.

(2) Dias, D.; Paulo Silva Cunha, J. Wearable Health Devices—Vital Sign Monitoring, Systems and Technologies. *Sensors* **2018**, *18*, 2414.

(3) Kalkal, A.; Kumar, S.; Kumar, P.; Pradhan, R.; Willander, M.; Packirisamy, G.; Kumar, S.; Malhotra, B. D. Recent advances in 3D printing technologies for wearable (bio)sensors, Addit. *Addit. Manuf.* **2021**, *46*, 102088.

(4) Choudhry, N. A.; Arnold, L.; Rasheed, A.; Khan, I. A.; Wang, L. Textronics—A Review of Textile-Based Wearable Electronics. *Adv. Eng. Mater.* **2021**, *23*, 2100469.

(5) Darabi, S.; Hummel, M.; Rantasalo, S.; Rissanen, M.; Öberg Månsson, I.; Hilke, H.; Hwang, B.; Skrifvars, M.; Hamedi, M. M.; Sixta, H.; Lund, A.; Müller, C. Green Conducting Cellulose Yarns for Machine-Sewn Electronic Textiles. *ACS Appl. Mater. Interfaces* **2020**, *12*, 56403−56412.

(6) Liang, A.; Stewart, R.; Freire, R.; Bryan-Kinns, N., Effect of bonding and washing on electronic textile stretch sensor properties, In *Adjunct Proceedings of the 2019 ACM International Joint Conference on Pervasive and Ubiquitous Computing and Proceedings of the 2019 ACM International Symposium on Wearable Computers*, ACM; 2019, pp. 121−124.

(7) Patel, P. C.; Vasavada, D. A.; Mankodi, H. R.; Applications of electrically conductive yarns in technical textiles, In *2012 IEEE International Conference on Power System Technology (POWERCON)*. IEEE; 2012.

(8) Zhao, J.; Fu, Y.; Xiao, Y.; Dong, Y.; Wang, X.; Lin, L. A Naturally Integrated Smart Textile for Wearable Electronics Applications. *Adv. Mater. Technol.* **2020**, *5*, 1900781.

(9) Meena, J. S.; Choi, S. B.; Jung, S.-B.; Kim, J.-W. Electronic textiles: New age of wearable technology for healthcare and fitness solutions. *Mater. Today Bio* **2023**, *19*, 100565.

(10) Liu, W.; Chang, Y.-C.; Zhang, J.; Liu, H. Wet-Spun Side-by-Side Electrically Conductive Composite Fibers. *ACS Appl. Electron. Mater.* **2022**, *4*, 1979−1988.

(11) Liu, W.; Liu, H.; Zhao, Z.; Liang, D.; Zhong, W.-H.; Zhang, J. A novel structural design of cellulose-based conductive composite fibers for wearable e-textiles. *Carbohydr. Polym.* **2023**, *321*, 121308.

(12) Qi, H.; Schulz, B.; Vad, T.; Liu, J.; Mäder, E.; Seide, G.; Gries, T. Novel Carbon Nanotube/Cellulose Composite Fibers As Multifunctional Materials. *ACS Appl. Mater. Interfaces* **2015**, *7*, 22404−22412.

(13) Ryan, J. D.; Mengistie, D. A.; Gabrielsson, R.; Lund, A.; Müller, C. Machine-Washable PEDOT: PSS Dyed Silk Yarns for Electronic Textiles. *ACS Appl. Mater. Interfaces* **2017**, *9*, 9045−9050.

(14) Yun, Y. J.; Lee, H. J.; Son, T. H.; Son, H.; Jun, Y. Mercerization to enhance flexibility and electromechanical stability of reduced graphene oxide cotton yarns. *Compos. Sci. Technol.* **2019**, *184*, 107845.

(15) Galante, A. J.; Haghanifar, S.; Romanowski, E. G.; Shanks, R. M. Q.; Leu, P. W. Superhemophobic and Antivirofouling Coating for Mechanically Durable and Wash-Stable Medical Textiles. *ACS Appl. Mater. Interfaces* **2020**, *12*, 22120−22128.

(16) Hasni, U.; Piper, M. E.; Lundquist, J.; Topsakal, E. Screen-Printed Fabric Antennas for Wearable Applications. *IEEE Open J. Antennas Propag.* **2021**, *2*, 591−598.

(17) Nomura, K.; Horii, Y.; Kanazawa, S.; Kusaka, Y.; Ushijima, H. Fabrication of a Textile-Based Wearable Blood Leakage Sensor Using Screen-Offset Printing. *Sensors* **2018**, *18*, 240.

(18) Verbič, A.; Gorjanc, M.; Simončič, B. Zinc Oxide for Functional Textile Coatings: Recent Advances. *Coatings* **2019**, *9*, 550.

(19) Wang, W.; Zhou, Z.; Liu, N.; Zhang, X.; Zhou, H.; Wang, Y.; Fang, K.; Wu, T. Improving Biocompatibility of Polyester Fabrics through Polyurethane/Gelatin Complex Coating for Potential Vascular Application. *Polymers* **2022**, *14*, 989.

(20) Berman, B. 3-D printing: The new industrial revolution. *Bus. Horiz.* **2012**, *55*, 155−162.

(21) McDonald, S., 3D printing: A future collapse-compliant means of production, In *Proceedings of the Second Workshop on Computing within Limits*, ACM; 2016, pp. 1−6.

(22) Ngo, T. D.; Kashani, A.; Imbalzano, G.; Nguyen, K. T. Q.; Hui, D. Additive manufacturing (3D printing): A review of materials, methods, applications and challenges. *Composites, Part B* **2018**, *143*, 172−196.

(23) Pasricha, A.; Greeninger, R. Exploration of 3D printing to create zero-waste sustainable fashion notions and jewelry. *Fash. Text.* **2018**, *5*, 30.

(24) Chang, Y.-C.; Shao, L.; Liu, W.; Bliss, B. J.; Zhao, B.; Zhao, Z.; Zhang, J. Unleashing the potential of waste: A supercharged high-performance 3D printing resin from discarded polylactic acid. *Chem. Eng. J.* **2024**, *489*, 151250.

(25) Shahrubudin, N.; Lee, T. C.; Ramlan, R. An Overview on 3D Printing Technology: Technological, Materials, and Applications. *Procedia Manuf.* **2019**, *35*, 1286−1296.
(26) Carradero Santiago, C.; Randall-Posey, C.; Popa, A.-A.; Duggen, L.; Vuksanovich, B.; Cortes, P.; Macdonald, E. 3D Printed Elastomeric Lattices With Embedded Deformation Sensing. *IEEE Access* **2020**, *8*, 41394−41402.
(27) Herren, B.; Saha, M. C.; Altan, M. C.; Liu, Y. Development of ultrastretchable and skin attachable nanocomposites for human motion monitoring via embedded 3D printing. *Composites, Part B* **2020**, *200*, 108224.
(28) Kim, T.; Yi, Q.; Hoang, E.; Esfandyarpour, R. A 3D Printed Wearable Bioelectronic Patch for Multi-Sensing and In Situ Sweat Electrolyte Monitoring. *Adv. Mater. Technol.* **2021**, *6*, 2001021.
(29) Li, K.; Wei, H.; Liu, W.; Meng, H.; Zhang, P.; Yan, C. 3D printed stretchable capacitive sensors for highly sensitive tactile and electrochemical sensing. *Nanotechnology* **2018**, *29*, 185501.
(30) MacDonald, E.; Wicker, R. Multiprocess 3D printing for increasing component functionality. *Science* **2016**, *353*, aaf2093.
(31) Nassar, H.; Khandelwal, G.; Chirila, R.; Karagiorgis, X.; Ginesi, R. E.; Dahiya, A. S.; Dahiya, R. Fully 3D printed piezoelectric pressure sensor for dynamic tactile sensing. *Addit. Manuf.* **2023**, *71*, 103601.
(32) Ramya, A.; *3D Printing Technologies In Various Applications*, https://www.semanticscholar.org/paper/3D-PRINTING-TECHNOLOGIES-IN-VARIOUS-APPLICATIONS-Ramya/8a7356c5296436ba664261f8eefc548c02e77cde. 2016, Accessed 19 March 2024.
(33) Wang, Z.; Gao, W.; Zhang, Q.; Zheng, K.; Xu, J.; Xu, W.; Shang, E.; Jiang, J.; Zhang, J.; Liu, Y. 3D-Printed Graphene/Polydimethylsiloxane Composites for Stretchable and Strain-Insensitive Temperature Sensors. *ACS Appl. Mater. Interfaces* **2019**, *11*, 1344−1352.
(34) Zhang, J.; Liu, E.; Hao, S.; Yang, X.; Li, T.; Lou, C.; Run, M.; Song, H. 3D Printable, ultra-stretchable, Self-healable, and self-adhesive dual cross-linked nanocomposite ionogels as ultra-durable strain sensors for motion detection and wearable human-machine interface. *Chem. Eng. J.* **2022**, *431*, 133949.
(35) Stuart, T.; Kasper, K. A.; Iwerunmor, I. C.; McGuire, D. T.; Peralta, R.; Hanna, J.; Johnson, M.; Farley, M.; LaMantia, T.; Udorvich, P.; Gutruf, P. Biosymbiotic, personalized, and digitally manufactured wireless devices for indefinite collection of high-fidelity biosignals. *Sci. Adv.* **2021**, *7*, No. eabj3269.
(36) Yin, X.-Y.; Zhang, Y.; Cai, X.; Guo, Q.; Yang, J.; Wang, Z. L. 3D printing of ionic conductors for high-sensitivity wearable sensors, Mater. *Horiz* **2019**, *6*, 767−780.
(37) Chen, J.; Zheng, J.; Gao, Q.; Zhang, J.; Zhang, J.; Omisore, O. M.; Wang, L.; Li, H. Polydimethylsiloxane (PDMS)-Based Flexible Resistive Strain Sensors for Wearable Applications. *Appl. Sci.* **2018**, *8*, 345.
(38) Gu, Z.; Wan, X.; Lou, Z.; Zhang, F.; Shi, L.; Li, S.; Dai, B.; Shen, G.; Wang, S. Skin Adhesives with Controlled Adhesion by Polymer Chain Mobility. *ACS Appl. Mater. Interfaces* **2019**, *11*, 1496−1502.
(39) Khatsenko, K.; Khin, Y.; Maibach, H. Allergic Contact Dermatitis to Components of Wearable Adhesive Health Devices. *Dermat. Contact Atopic Occup. DruDermatitisg* **2020**, *31*, 283−286.
(40) Korger, M.; Glogowsky, A.; Sanduloff, S.; Steinem, C.; Huysman, S.; Horn, B.; Ernst, M.; Rabe, M. Testing thermoplastic elastomers selected as flexible three-dimensional printing materials for functional garment and technical textile applications. *J. Eng. Fibers Fabr.* **2020**, *15*, 1558925020924599.
(41) Liu, J.; Jiang, S. Wearable properties of polylactic acid and thermoplastic polyurethane filaments 3D printed on polyester fabric. *J. Ind. Text.* **2023**, *53*, 152808372311663.
(42) Kim, I.; Shahariar, H.; Ingram, W. F.; Zhou, Y.; Jur, J. S. Inkjet Process for Conductive Patterning on Textiles: Maintaining Inherent Stretchability and Breathability in Knit Structures. *Adv. Funct. Mater.* **2019**, *29*, 1807573.
(43) Kim, J.; Kumar, R.; Bandodkar, A. J.; Wang, J. Advanced Materials for Printed Wearable Electrochemical Devices: A Review. *Adv. Electron. Mater.* **2017**, *3*, 1600260.
(44) Wu, S.; Zeng, T.; Liu, Z.; Ma, G.; Xiong, Z.; Zuo, L.; Zhou, Z. 3D Printing Technology for Smart Clothing. *A Topic Rev. Mater.* **2022**, *15*, 7391.
(45) Ching, T.; Li, Y.; Karyappa, R.; Ohno, A.; Toh, Y.-C.; Hashimoto, M. Fabrication of integrated microfluidic devices by direct ink writing (DIW) 3D printing. *Sens. Actuators, B* **2019**, *297*, 126609.
(46) Gao, C.; Xing, T.; Hou, X.; Chen, G. The influence of ink viscosity, water and fabric construction on the quality of ink-jet printed polyester. *Color. Technol.* **2020**, *136*, 45−59.
(47) Yuk, H.; Zhao, X. A New 3D Printing Strategy by Harnessing Deformation, Instability, and Fracture of Viscoelastic Inks. *Adv. Mater.* **2018**, *30*, 1704028.
(48) Kotek, R.; Afshari, M.; Avci, H.; Najafi, M.. *7 - Production of polyolefins*; 2nded, Woodhead Publishing, 2017, pp. 189−264.
(49) Smits, F. M. Measurement of Sheet Resistivities with the Four-Point Probe, Bell Syst. *Technol. J.* **1958**, *37*, 711−718.
(50) Han, W.; Wu, Y.; Gong, H.; Liu, L.; Yan, J.; Li, M.; Long, Y.; Shen, G. Reliable sensors based on graphene textile with negative resistance variation in three dimensions. *Nano Res.* **2021**, *14*, 2810−2818.
(51) Kol, R.; De Somer, T.; D'hooge, D. R.; Knappich, F.; Ragaert, K.; Achilias, D. S.; De Meester, S. State-Of-The-Art Quantification of Polymer Solution Viscosity for Plastic Waste Recycling. *ChemSuschem* **2021**, *14*, 4071−4102.
(52) Guo, Z.; Fei, F.; Song, X.; Zhou, C.;. Analytical Study of Shear-Thinning Fluid Flow in Direct Ink Writing Process, In *American Society of Mechanical Engineers Digital Collection*; ASME; 2022.
(53) Wei, P.; Cipriani, C.; Hsieh, C.-M.; Kamani, K.; Rogers, S.; Pentzer, E. Go with the flow: Rheological requirements for direct ink write printability. *J. Appl. Phys.* **2023**, *134*, 100701.
(54) Li, X.; Zhang, P.; Li, Q.; Wang, H.; Yang, C. Direct-ink-write printing of hydrogels using dilute inks. *iScience* **2021**, *24* (4), 102319.
(55) Papakonstantinou, D.; Amanatides, E.; Mataras, D.; Ioannidis, V.; Nikolopoulos, P. Improved Surface Energy Analysis for Plasma Treated PET Films, Plasma Process. *Polymer* **2007**, *4*, S1057−S1062.
(56) Liu, Z.; Fang, K.; Gao, H.; Liu, X.; Zhang, J. Effect of cotton fabric pretreatment on drop spreading and colour performance of reactive dye inks, Color. *Technol* **2016**, *132*, 407−413.
(57) Salavagione, H. J.; Sherwood, J.; Bruyn, M. D.; Budarin, V. L.; Ellis, G. J.; Clark, J. H.; Shuttleworth, P. S. Identification of high performance solvents for the sustainable processing of graphene. *Green Chem.* **2017**, *19*, 2550−2560.
(58) Ferrero, F.; Periolatto, M.. *Modification of Surface Energy and Wetting of Textile Fibers*; Wetting Wettability, 2015.
(59) Das, B.; Das, A.; Kothari, V. K.; Fanguiero, R.; Araújo, M. D. Moisture Transmission Through Textiles. *Autex Res. J.* **2007**, *7*, 100−110.
(60) Ito, H.; Muraoka, Y. Water Transport Along Textile Fibers as Measured by an Electrical Capacitance Technique. *Text. Res. J.* **1993**, *63*, 414−420.
(61) Bormashenko, E. Progress in understanding wetting transitions on rough surfaces. *Adv. Colloid Interface Sci.* **2015**, *222*, 92−103.
(62) Hollies, N. R. S.; Kaessinger, M. M.; Bogaty, H. Water Transport Mechanisms in Textile Materials1 Part I: The Role of Yarn Roughness in Capillary-Type Penetration. *Text. Res. J.* **1956**, *26*, 829−835.
(63) Sánchez-Balderas, G.; Velázquez, J. D. H.; Pérez, E. Dependence of the Liquid Polarity in the Wetting of Rough Surface: An Effective Surface Tension Approach. *Langmuir* **2022**, *38*, 12804−12812.
(64) Shim, M. H.; Kim, J.; Park, C. H. The effects of surface energy and roughness on the hydrophobicity of woven fabrics. *Text. Res. J.* **2014**, *84*, 1268−1278.
(65) Seyedin, S.; Zhang, P.; Naebe, M.; Qin, S.; Chen, J.; Wang, X.; Razal, J. M. Textile strain sensors: A review of the fabrication

https://doi.org/10.1021/acsomega.4c11367
ACS Omega 2025, 10, 14138−14149

technologies, performance evaluation and applications, Mater. *Horiz* **2019**, *6*, 219−249.
(66) Kouchakzadeh, S.; Narooei, K. Simulation of piezoresistance and deformation behavior of a flexible 3D printed sensor considering the nonlinear mechanical behavior of materials, Sens. *Actuators Phys.* **2021**, *332*, 113214.
(67) Zhang, Z.; Xiang, D.; Wu, Y.; Zhang, J.; Li, Y.; Wang, M.; Li, Z.; Zhao, C.; Li, H.; Wang, P.; Li, Y. Effect of Carbon Black on the Strain Sensing Property of 3D Printed Conductive Polymer Composites, Appl. *Compos. Mater.* **2022**, *29*, 1235−1248.
(68) Felisberto, M.; Arias-Durán, A.; Ramos, J. A.; Mondragon, I.; Candal, R.; Goyanes, S.; Rubiolo, G. H. Influence of filler alignment in the mechanical and electrical properties of carbon nanotubes/epoxy nanocomposites. *Phys. B Condens. Matter* **2012**, *407*, 3181−3183.
(69) Goh, P. S.; Ismail, A. F.; Ng, B. C. Directional alignment of carbon nanotubes in polymer matrices: Contemporary approaches and future advances, Compos. *Part Appl. Sci. Manuf.* **2014**, *56*, 103−126.
(70) Irfan, M. S.; Ali, M. A.; Khan, K. A.; Umer, R.; Kanellopoulos, A.; Abdul Samad, Y. An electronic textile embedded smart cementitious composite. *Eng. Rep.* **2022**, *4*, No. e12468.

https://doi.org/10.1021/acsomega.4c11367
ACS Omega 2025, 10, 14138−14149